DIAGNOSTICS FOR HIGH POWER ACCELERATOR MACHINE PROTECTION SYSTEMS*

S. Lidia[#], Facility for Rare Isotope Beams, Michigan State University, East Lansing, MI, USA

Abstract

Modern hadron accelerators create and transport beams that carry MW-scale power or store GJ-scale energy. The Machine Protection Systems (MPS) that guard against both catastrophic failures and long-term performance degradation must mitigate errant beam events on time scales as short as several microseconds. Measurement systems must also cope with detection over many orders of magnitude in beam intensity to adequately measure and respond beam halo loss. Other issues, such as radiated signal cross-talk, also confound and complicate delicate measurements. These requirements place enormous demands on the MPS beam diagnostics and beam loss monitors. We will review the current state of MPS diagnostic systems for this class of accelerator, including SNS, ESS, FRIB, LHC, J-PARC, and SPIRAL-II. Specific designs and key performance results will be presented and discussed.

INTRODUCTION

Trends in modern accelerators push at the boundaries of beam energy (LHC, ILC), beam power (Fig. 1) and brightness [1][2]. Accelerator based neutron-generating facilities (SNS, JPARC, PSI, LANSCE) have pushed the frontier of proton beam power to 1 MW, with 5 MW beams in development [ESS]. For heavy ion beams, the frontier will be advanced by more than two orders of magnitude to 400 kW at FRIB [FRIB]. High energy hadron colliders have pushed the frontier of stored proton beam energy from 1-3 MJ (SPS, RHIC, HERA, TEVATRON) to 140 MJ (LHC, design goal 360 MJ).

Key technology development has powered the push at high intensity frontier [1]. Continuing improvements in SRF accelerator and large-scale cryogenics enable efficient, high gradient acceleration and robust operation. Ion source, RFQ, and low energy beam transport produce intense, high charge state, high brightness, CW beams. High power charge strippers and beam collimators accept many kWs of beam power. Rapid-cycling booster synchrotrons accept and accumulate high intensity beams and then accelerate with minimal losses. High power beam targets and radiation resistant magnets operate are necessary to handle the intense thermal and radiation fields generated. Finally, loss detection and machine protection techniques are crucial to prevent damage from prompt, fast events and to monitor and control chronic losses from small ($<10^{-4}$-10^{-6}) fractions of the beam power.
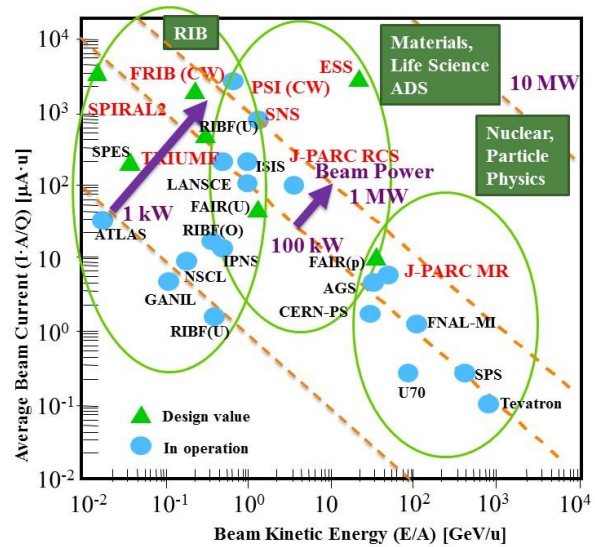
Figure 1: Development of high power hadron accelerators. [1].

MACHINE PROTECTION SYSTEM BASICS

Machine protection systems exist to avoid prompt and long-term damage to the accelerator and experimental instrumentation, to minimize the number of false trips that limit production, and to provide evidence of failures or fault events when interlock systems stop beam operation [3][4].

Machine failures can derive from several sources. Hardware failures can include power supply trips, magnet or cavity quench, RF trips and low-level control loss, loss of vacuum, etc. Control system failures include incorrect calibrations and settings updates, trigger mistiming and timing distribution errors, feedback malfunctions. Operational sources include tuning and steering errors, and administrative controls on beam mode and machine state. Beam instabilities at high current or high brightness can develop quickly and damage components.

The time response for MPS interdiction ranges over many orders of magnitude. Fast protection systems (FPS) serve to protect against prompt damage from beam impacts. Typical FPS response times can vary from several to some hundreds of microseconds, and reflect thermodynamic changes of accelerator materials caused by errant beams. Run permit systems (RPS) operate on a slower time scale, from milliseconds to many seconds, typically, and are used to verify machine state and identify conditions that may lead to unintended damage or long term irradiation effects that limit personnel access. As accelerator facilities may function

in many different operating modes with varying thresholds for beam induced damage, the complete machine protection system must be flexible and configurable.

Accelerator Prompt Damage Capacities

Hadron beam loss effects in materials depend strongly on species, energy, and intercepting materials. High energy hadrons (greater than some 100's GeV/u) can generate cascades of secondary particles that lead to deep (several m) penetration and energy deposition. Material damage as well as quenching of cryogenic components can occur.

Lower energy hadron beams (10's to 100's MeV/u) deposit their energy primarily on the surface of components, which can lead to local temperature increase. Plastic deformation and rapid melting can occur when the energy deposition exceeds 10 kJ. Penetration range of low and medium energy hadrons is shown in Fig. 2 below.
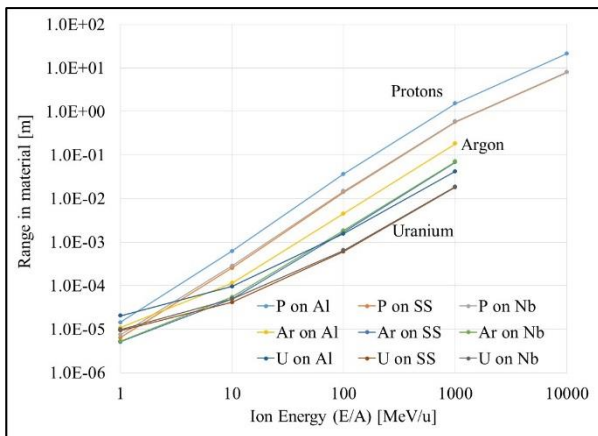

Figure 2: Penetration range for H, Ar, and U ions onto Al, stainless steel, and Nb from SRIM [5].

The time to failure for beamline components is necessary to understand in order to define the MPS fast response requirements. Figure 3 shows the time to failure of Nb and stainless components in the FRIB complex [6][7] when U ions are accelerated. ANSYS [8] calculations of energy deposition, thermal transport, and material stress.

In SRF cryomodules, power losses can generate additional heat load and induced quenches. Particle losses on or near SRF cavity surfaces can degrade the surface resistance, introduce defects and field emission sites, and affect the local gas distribution. These latter effects can degrade the operational gradient of the cavity by lowering the cavity Q-factor, and interfere with the low-level operation of the cavity rf controls.

MPS Fast Detection Times

The required detection time scales for errant beam detection in existing and proposed high power facilities are shown in Table 1. Current development of machine

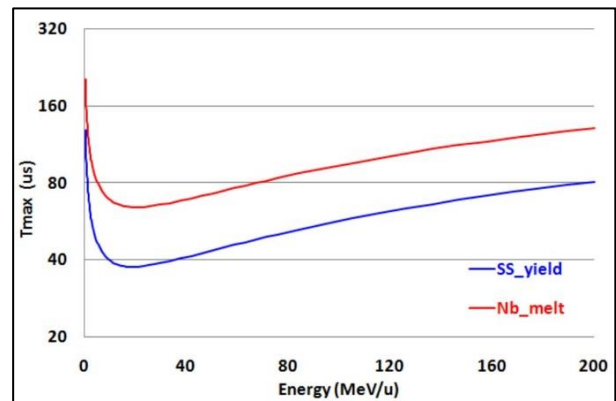protection systems require 'not OK' signals to be generated within 1-10 µs.

Figure 3: Time to failure for Nb and stainless steel components driven by 2mm, 8.4 pµA U beam. [6]

Table 1: Errant Beam Detection Time Scale Limits

	Ion	Energy [MeV/u]	Beam Power [MW]	Detection time limit [µs]
PSI	H$^+$	590	1.3	few 100
SNS	H$^-$/H$^+$	1000	1-2	5-10
ESS	H$^-$/H$^+$	2000	5	1-2
SPIRAL-2	D/HI	20	0.2	10
FRIB	HI	200	0.4	10
JPARC-MR	H+	3×10^4	0.75	10
LHC	H$^+$	7×10^6	4×10^6	80

Slow Loss Generation and Detection

Slow beam losses can be generated when the tails of the beam distribution are intercepted at the vacuum chamber walls, when primary beam particles scatter from residual gases, and other causes. These chronic, low-level losses lead to activation of components and limit access to the beam line.

Previous experience at high power facilities [9] [10] have indicated that a loss of 1 W/m corresponds to activation levels about 100 mR/hr. More recent measurements at SNS [11] (Fig. 4) have demonstrated activation rates of 30-40 mR/hr corresponding to beam power ~1 MW. This can be compared to the LANSCE experience of 100 mR/hr with 780 kW beam power.
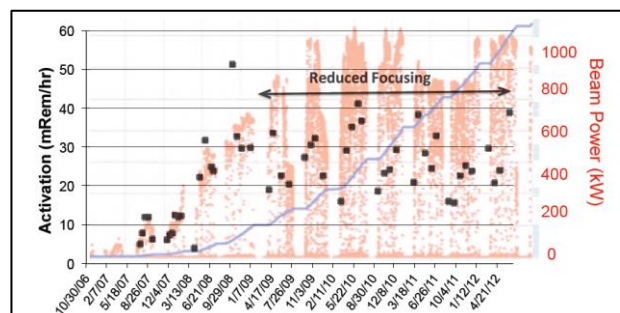

Figure 4: Residual activation in the SNS SCL [11].

At most facilities, the baseline detection and background requirements are set in the range 0.5-1 W/m. Improvements in beam orbit and halo control, and improved detection thresholds are sought to decrease the slow loss rates to 0.1 W/m or lower.

Challenges and Opportunities

There are significant issues and multiple areas for diagnostic development in support of machine protection systems at contemporary high intensity hadron machines: development of systems with high dynamic range sensitivity that must contend with high radiation fields and EMI environments; development of fast and robust reporting and control networks, with low false-trip rates; simulations and modelling of radiation fields from slow and prompt beam losses, and the distribution of loss patterns from specific fault events.

QUANTITIES MEASURED WITH DIAGNOSTIC INSTRUMENTATION

Various quantities are utilized as inputs to the machine protection system. These parameters measure and gauge the behaviour of the beam and the performance of accelerator components, and compare against known or anticipated thresholds.

Beam loss monitors are employed to directly monitor the prompt radiation fields produced by the accelerator components (eg. rf cavities, distribution lines and sources) as well as the secondary particle fields generated by primary beam impact onto the vacuum chamber walls. Gamma and neutron detectors are common in medium to high energy facilities. Techniques to detect hadronic showers can also be useful in that they may indicate threshold energy levels in primary beams, and may be more advantageously staged further from the vacuum chamber.

Direct beam measurements will indicate normal or errant behavior that may require interdiction of the beam, by dumping the stored beam and preventing the source chain from injecting or producing new beam, until the problem is resolved. Specific beam measurements include average and peak current (intensity), beam orbit, beam halo, micro pulse duration, and spot size.

Vacuum monitoring is critical to preserve the operational lifetime of superconducting rf (SRF) cavities. Vacuum gauges are employed for leak detection as well as for any slow changes in the background gas pressure due to beam (and secondary) particle impacts on the vacuum chamber walls.

Cryogenic system monitors are used to detect changes in the overall thermal loading budget, indicating changes in source terms. Heat load source changes can result from changes in forward or reflected rf power (and the formation of standing waves in distribution lines), increased radiative heat loads in cryogenic devices due to changes in rf beam loading, and from beam particle

interception on limiting apertures. Quench detection circuits monitor for changes in the superconducting state of magnet windings, or the Q-factor of SRF cavities. Low-level rf (LLRF) digital monitors are employed to detect fast (~µs) changes in SRF cavity field amplitudes, forward/reflected power, and phase.

Normal conducting magnet power supplies are typically monitored with DC current transformers (DCCTs) that detect changes in supplied current to magnet coils, which may result in changes to the beam orbit or focusing. Changes to DCCT readings may interlock the beam.

PROMPT RADIATION GENERATION ALONG ACCELERATOR CHAIN

Radiation production along the accelerator chain exhibits derives from several sources.

Background sources of gamma radiation are produced by high field rf cavities, couplers, transmission lines and rf sources. These photons interact with detectors, vacuum chamber walls and other components to generate electrons and increase overall background noise levels. Measured background levels can be in excess of 1 Rem/hr [12][13].
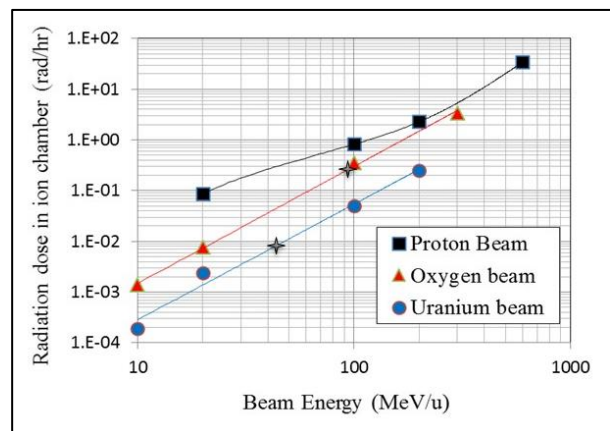

Figure 5: Gamma ray dose at 30cm from cryomodule. Power loss is normalized to 1 W/m. Pencil beam with 3mrad angle was uniformly distributed along 150m long linac segment.[12]

Beam induced radiation fields include gamma, neutron, and hadronic cascades. The fields are produced when a primary beam particle collides with the vacuum chamber, insertable diagnostics, or background gas molecules. The production rates are strongly dependent on primary beam energy.

Gamma ray doses generated with several hadron beams in the FRIB accelerator, modelled by GEANT4 [14], are shown in Fig. 5. The beam losses are assumed to be 1 W/m distributed uniformly along a 150-m linac section. For heavy ion beams, the prompt gamma radiation dose can easily be masked by background gamma sources at beam energies below a few 100s MeV/u.
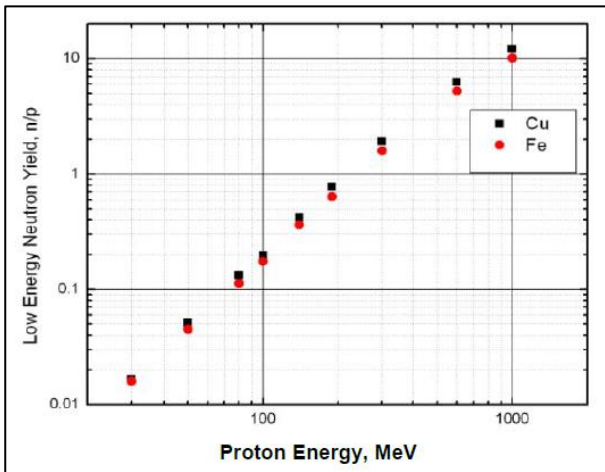
Figure 6: Evaporation neutron yield from a copper target as a function of incident proton energy. [15]

The collision of high energy hadron beams with beamline components and background gases precipitates various nuclear interactions. Neutron evaporation [16] is the main source of neutrons in hadron machines. Low energy neutron transport processes [17] describe the propagation and thermalization of neutrons in materials and detectors. Neutron production rates from evaporation processes of protons onto copper and iron are shown in Fig. 6. Neutron fluxes from heavy ion beam losses (uniform 1W/m) also exhibit energy and species dependence (Fig. 7).
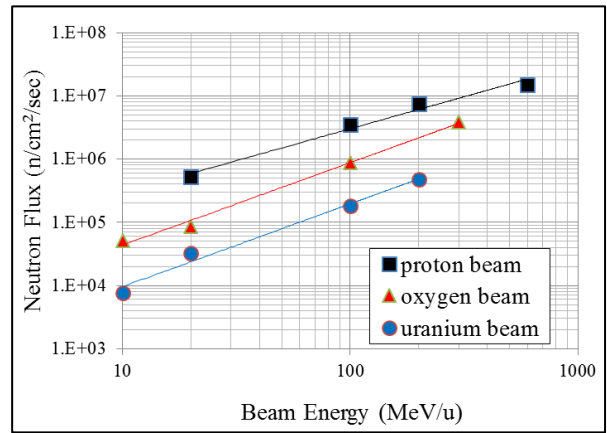

Figure 7: Neutron flux normalized to 1W/m loss. [12].

Hadronic cascades or showers generate a mixed radiation field of gammas, lepton, and hadrons. These showers can, in principle, be modeled with Monte Carlo codes [14][18][19][20][21]. A recent benchmark study [22] was performed at the CERN-EU High Energy Reference Field Facility (CERF) to calibrate LHC beam loss monitors. FLUKA generated spectra were presented in [23], Fig. 8 below.
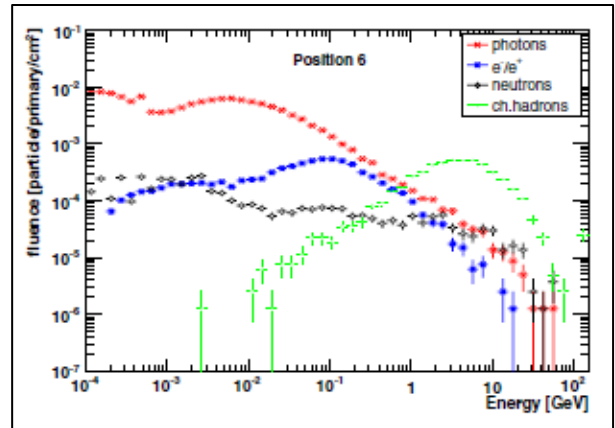

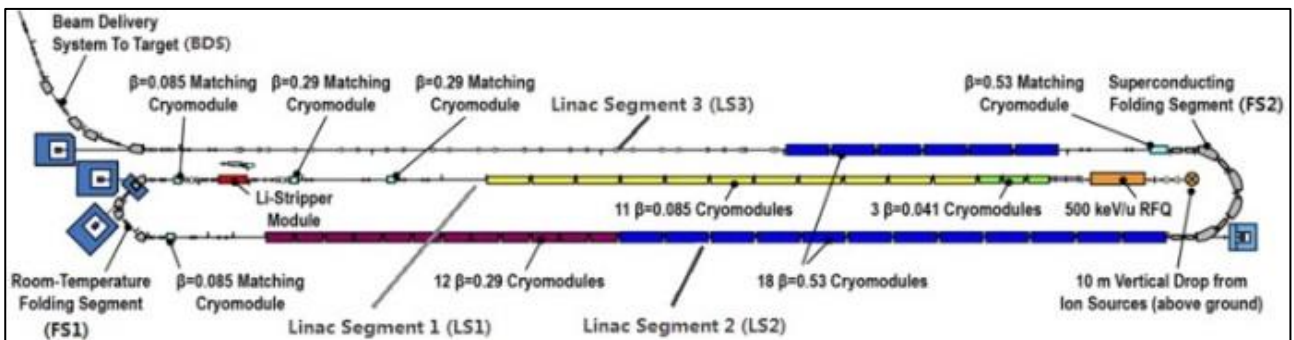Figure 8: FLUKA hadron spectra from high energy proton beam bombardment [23].

Figure 9: FRIB drive accelerator layout, showing the folded, 'paperclip' geometry.

Crosstalk Effects

Compact, low energy, high intensity hadron accelerators, especially those attached to existing campuses or facilities, can encounter crosstalk issues when the higher energy portions of the beamline are brought into close proximity with the lower energy portions. A current example is the 'paperclip' design of the FRIB drive linac, Fig. 9.

In the FRIB case, the drive linac is separated into 3 segments, with the lowest energy segment (LS1) placed between the two higher energy ones (LS2, LS3). Uniform beam losses of 1 W/m have been simulated with GEANT [14] and PHITS [19]. Figure 5 shows the gamma radiation dose rate at 30 cm from the cryomodule. The crosses indicate the strength of the radiation field at LS1 due to losses occurring in LS3. At these beam loss rates, ionization chambers along LS1 would be overwhelmed by signal from LS3. A similar situation exists for the neutron field, where the LS3 signal detected at LS1 exceeds the LS1 signal by ~30 times (Fig. 10).
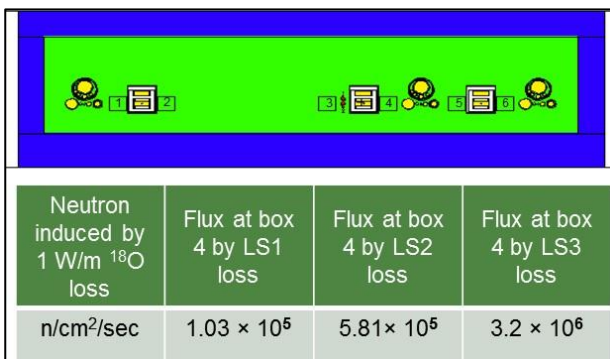

Neutron induced by 1 W/m ^{18}O loss	Flux at box 4 by LS1 loss	Flux at box 4 by LS2 loss	Flux at box 4 by LS3 loss
n/cm^2/sec	1.03×10^5	5.81×10^5	3.2×10^6

Figure 10: Neutron crosstalk effects in FRIB linac, modeled with PHITS [12]. The top figure shows a cross section of the beamline.

SIMULATIONS AND MODELING

The design, development, and implementation of diagnostic systems for machine protection require extensive evaluation of fault modes, risk analyses, and beam loss events and spill patterns.

Predicted radiation power levels from low level beam spill processes can be modelled with radiation transport codes [14][18[19][20][21] (Fig. 11) to estimate dose rates at various sections of the machine.

To assess risk from infrequent, prompt fault events due to component failure or mistuning, beam spill patterns need to be generated and analyzed [25][26][27]. Spill pattern maps (Fig. 12) can aid in the placement of in-vacuum diagnostics and passive protection devices to limit damage to sensitive components.
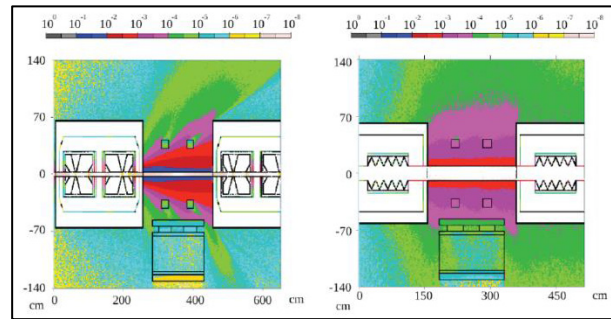

Figure 11: Radiation field power density (Gy/sec) in the ESS linac from uniform 1 W/m losses at 200 MeV (left) and 2 GeV (right) [24].

Once constructed, a comprehensive atlas of spill pattern maps can be incorporated into a machine learning framework [25][28] to optimize the placement of beam loss monitors and their networking, and in the post-mortem analysis of fault events.
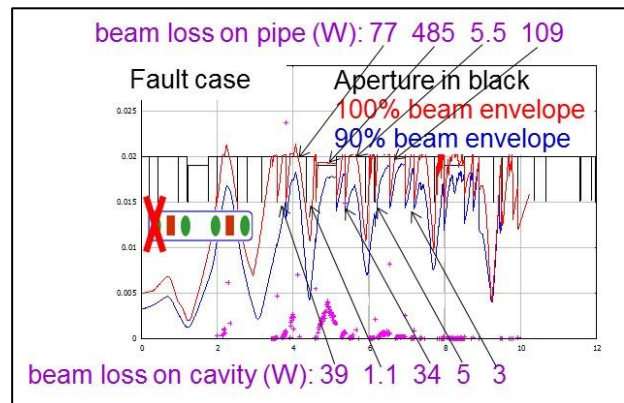

Figure 12: Beam loss map in the FRIB linac due to single cavity failure. [26].

BEAM LOSS MONITORS

We describe various beam loss monitor instrumentation techniques currently employed at high power facilities. This follows the excellent tutorial by Zhukov [15].

Ionization Chambers

Ion chambers are the main type of loss monitors used in hadron machines. These are gas-filled chambers containing an electrode pair with applied high voltage. Multiple ion chambers are typically strung together on a common high voltage supply. When operated in the ionization mode, the chamber sensitivity is largely insensitive to HV fluctuations.

Small ion chambers (Fig. 13) have been designed and optimized for various machines. The SNS ionization chamber [29] has a volume of 133 cm^3 of argon gas. At a HV bias of -2 kV the chamber sensitivity is 70 nC/rad. The response time for charge collection can be ~1-2 μs.

Figure 13: SNS type ionization chamber. [29]

A larger chamber developed for LHC [30] is shown in Fig. 14. The LHC chamber was developed in collaboration with the Institute for High Energy Physics (Protvino, Russia). The detector is filled with N_2 at 100 mbar overpressure. The 50-cm-long, 9-cm-diameter chamber is constructed with parallel aluminium plates, separated by 0.5 cm. The 1.5 L volume provides a sensitivity of ~54 μC/Gy at 1500 V bias. The response time is approximately 300 ns for electrons and 80 μs for ions. The electron mode is compatible with fast detection requirements for high intensity hadron machines.

Figure 14: The LHC ionization chamber. [30]

Secondary Emission Monitors

At locations with very high loss rates, the high sensitivity of the ion chambers can lead to saturation and charge pile-up. Secondary emission monitors (Fig. 15) exhibit lower sensitivity, thus extending the detection dynamic range when used to complement ionization chambers. The center electrode of the 3-electrode is titanium rather than aluminium to take advantage of the greater stability of the secondary emission coefficient with integrated radiation dose [31].
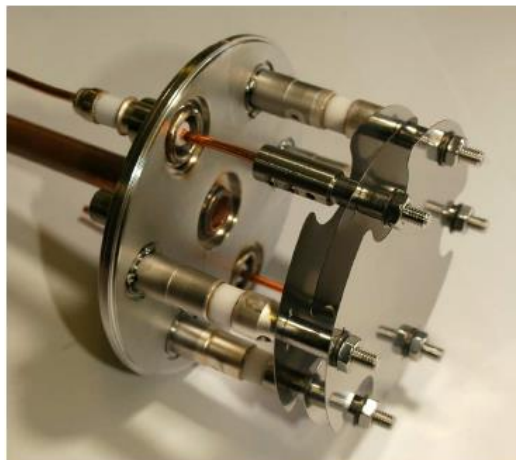

Figure 15: Secondary emission chamber developed for LHC magnet quench protection.[32].

Scintillation-Based Detectors

Scintillation based schemes typically employ photomultiplier tubes that increase gain by 10^5-10^8 with applied HV. The wide variety of scintillation materials available allow for optimization to detect specific types of radiation. Many crystalline and powder scintillating materials [33] have excellent efficiencies at gamma detection, with decay time constants mostly in the 10s-100s ns. Pulse shape discrimination of the waveform is used to separate gamma and neutron signals. Plastic based scintillator materials containing ^{6}Li or ^{10}B are widely used to detect fast and thermal neutrons. These latter types are useful for discriminating neutron-producing beam losses from background gamma sources. Moderated detectors are relatively slow, but are sensitive to neutron fluxes over a wide range, 10^4-10^8 n/cm^2/s for the SBLM [34], suitable for monitoring slow beam losses.

Background Subtraction

Overall sensitivity to beam losses can be improved with background subtraction techniques. These can be implemented in hardware, software, or firmware. Dual beam loss monitors [34] are utilized that provide differential sensitivity to background gammas and beam-induced neutron signals. Beam loss monitor signals can also be acquired at rates that permit the discrimination between 'beam on' and 'beam off' events. Robust background subtraction can then be performed in software (see Fig. 16), which limits the time response to seconds. Firmware implementation can reduce the comparison time against a stored background waveform and recover μs-scale responsivity.
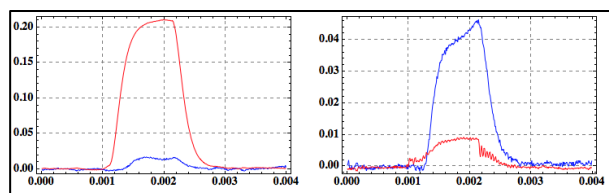

Figure 16: Background subtraction of SNS BLM waveforms, performed in software. Red traces are RF only waveforms, blue traces are beam loss only (ie. subtracted). [34]

Novel Schemes for In-Situ Cryogenic Detection

Detection of beam losses inside of cryomodules is critical to minimize damage to sensitive cavity surfaces, and to prevent quenching of magnets with large stored energy.

Recent work at LHC [35][46] have studied the feasibility of using silicon (300 μm) and CVD diamond (500 μm) in the cold mass at 1.9K to measure slow losses with sensitivities 0.1-10 mGy/s and response times <1 ms. Measured response times to Minimum Ionizing Particles (MIPS) were 2.5 ns and 3.6 ns for silicon and diamond, respectively, at liquid helium

temperatures, allowing bunch by bunch resolution. Signal reduction factors were measured and calibrated to the expected LHC 20 year integrated dose (2 MGy). The expected degradation factor is 25 for silicon and 14 for diamond.

A system based on collection of charge carriers in liquid helium itself was also considered, as the material is self-healing and does not exhibit degradation from integrated dose. With an applied electric field of 200 V/mm, sensitivity of ~0.1 fC/cm/MIP was measured. Slow charge collection limits the time response to events longer than ~200 μs. A similar system has been developed and employed at Fermilab [37] (Fig.17).
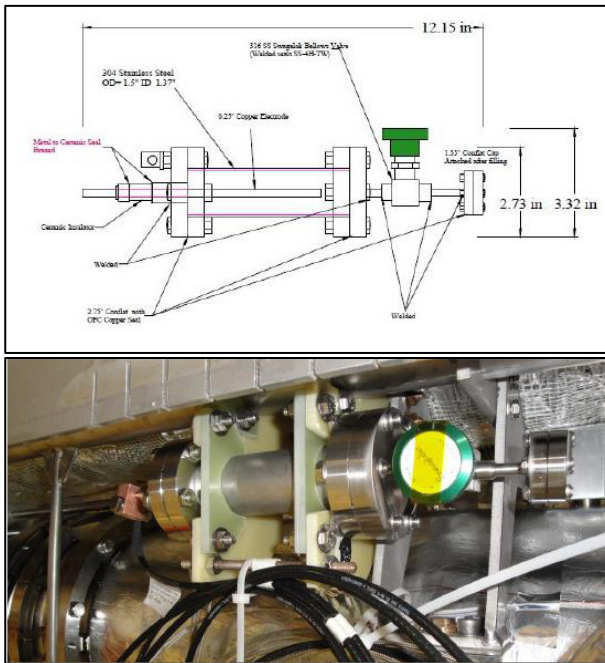

Figure 17: Cryogenic ionization chamber at ASTA [37].

Systems employing fast thermometry or calorimetry have been developed to monitor the temperature of cryogenic components and beamlines [38][39]. Resistance temperature detectors (Cernox RTDs) are employed to monitor the surface temperature of components.

Fast thermometry techniques are currently being explored to detect low level, slow beam losses at limiting apertures in cryomodules. ANSYS models can be used to predict the change in component temperature and time rate under beam thermal loading conditions (Table 2).

Table 2: Cryogenic Beam Loading Response

Rising time for 0.1K temperature difference from beam loss		
Beam loss in cryomodule	0.1 W/m	1 W/m
0.1K rising time	1 min	7 sec
Maximum temperature rising	1.83 K	8.9 K
Total rising time	30 min	20 min

Initial measurements of thermal loading and RTD pickups were conducted at FRIB [40]. Initial sensor response is encouraging for detection of several mK temperature rise with a time response of 10's seconds. Improvements to the sensitivity and time response are expected with higher sampling and averaging rates (1-10kHz).

DIRECT BEAM DIAGNOSTICS FOR FAST TIME SCALES

The measurement of beam properties themselves, on a suitably fast basis, can directly inform the machine protection system to cease beam production and to dump stored beam. Robust monitoring of beam current at the 1-10% level of the normal current on a fast time scale (several μs) is generally required to detect changes in the beam intensity that may require MPS interdiction. Beam position monitors, capacitive pickups, and current sensing interceptive devices near the limiting beam aperture can also provide reliable detection sensitivity. Modern FPGA electronics systems are gaining wide acceptance for fast and flexible beam loss detection and interface to MPS decision and control systems.

Beam Current Monitors (BCM)

Most current sensing of intense beams is conducted with AC or DC current transformers (ACCT, DCCT) with appropriate analog front end, analog-to-digital conversion, and digital signal processing (Fig. 18).
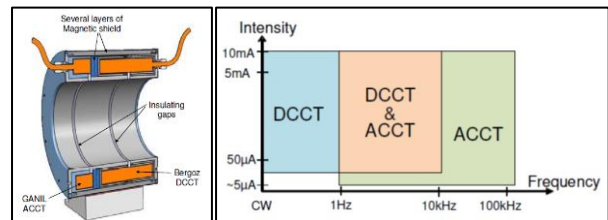

Figure 18: Hybrid ACCT/DCCT developed for SPIRAL-2 (left) and frequency response for DCCT and ACCT systems (right).[41].

The differences between ACCTs and DCCTs have important implications to their optimal use for tuning and MPS. DCCTs require offset correction and are limited in their high frequency response to slower current evolution (100s μs). However, they can more easily the presence and absence of beam. ACCTs have higher frequency response, and so can detect relatively fast changes in beam current (<10 μs), but they have no DC response and so must be periodically re-baselined to define the 'no current' condition. Additional signal conditioning is required to compensate for current 'droop' in the time response. [42]

Differential Beam Current Monitoring (DBCM)

The fast response of ACCTs has led to a demonstration of a fast MPS network to detect errant

beams on the SNS linac [43], based on differential beam current monitoring (DBCM) between two spatially separated locations (Fig. 19).
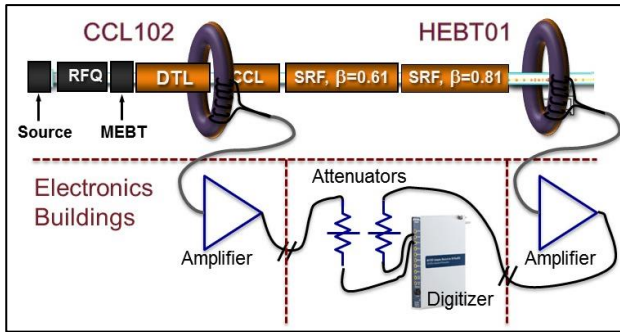

Figure 19: SNS differential beam current monitor.[43].

The SNS configuration consists of two wideband (1 GHz, 1 ms droop time constant) current transformers, and relatively long cable lengths (500-1200ft). The electronic platform consists of PXIe real-time controller with FlexRIO FPGA and 14-bit, 2-channel, 100MS/s digitizer. The FPGA processing performs the time-of-flight accounting for the beam and cable lengths, applies calibrations and corrects for drifts and droop in the transformer. The block diagram of the digital processing and interface with the MPS control is shown in Fig. 20.
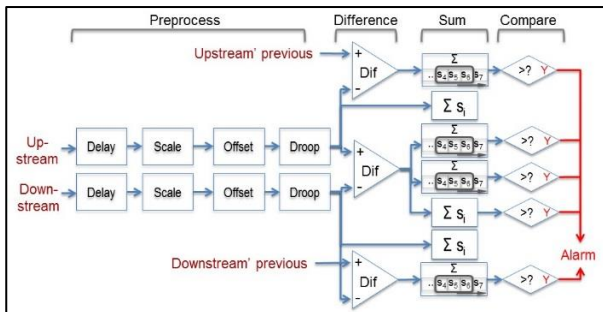

Figure 20: Digital processing of SNS DBCM. [43].

Similar systems are proposed for ESS, SPIRAL-2, and FRIB. In the SPIRAL-2 implementation the MPS control is based on a preset beam charge loss threshold rather than a beam intensity threshold [44]. The distribution of DBCM monitors for SPIRAL-2 is shown in Fig. 21, and the proposed distribution for FRIB in Fig. 22. The ESS implementation has been bench tested with a measured response time of 770 ns. Including additional delays from the analog electronics, digital filters and rear transition module to the μTCA chassis, the expected response time still meets the required 1-2 μs [45].
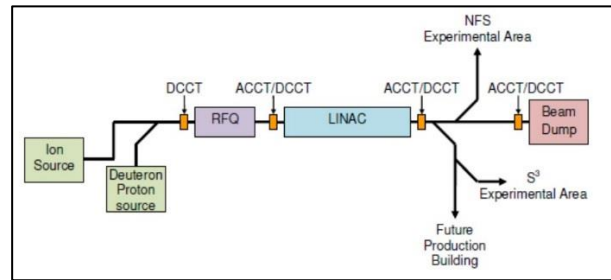

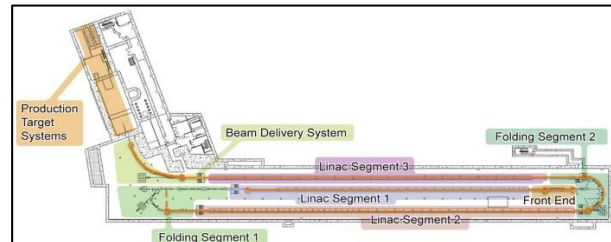Figure 21: Distribution of beam current monitors in SPIRAL-2. [41].

Figure 22: Distribution of beam current (open circles) in FRIB. [46].

Beam Position Monitors (BPM)

Beam position monitors are currently being developed and implemented in MPS applications. Besides fast orbit monitoring and deviation detection, recent studies at SNS have indicated how to include BPMs as part of a differential intensity monitoring system [47].

The SNS BPM current measurement scheme utilizes the digital sum signal from the four BPM capacitive sensors. The signal is processed within the FPGA to reconstruct the signal amplitude from the logarithmic amplifier. A final calibration is applied based on an existing BCM reference. The BPM and BCM signals are shown in Fig. 23.
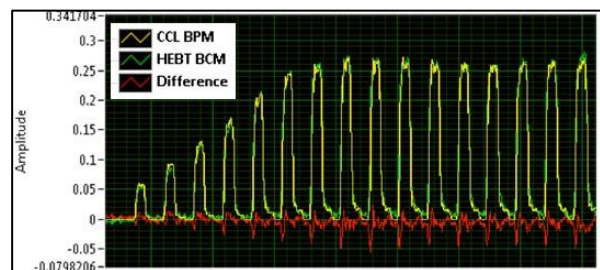

Figure 23: Cross-calibration of BPM and ACCT for differential intensity monitoring. [47].

Utilizing BPMs as intensity monitoring devices, and incorporating them into differential intensity monitoring schemes significantly increases the density of the monitoring network. However, limited linear apertures in the BPMs as well as low-beta effects [48] can increase the complexity of the required signal analysis, making the practical implementation of BPMs as intensity monitors problematic. Recent work has addressed possible schemes for implementing low-beta corrections [49].

Halo or Loss Monitor Rings

Beam loss monitors based on radiation detection have limited sensitivity for low energy hadron beams (< 20 MeV/u). The FRIB design increases the problems for low energy beam loss detection by placing the lowest energy linac in close proximity to the highest energy linac. In this case, both ionization chamber and neutron detector instruments at the low energy side are swamped with signal from slow losses from the high energy linac.

The halo, or loss, monitor ring was designed as a minimally interceptive device [13], with high sensitivity (~0.1 nA) to small losses and fast response (<15 μs) for large losses. The device is designed to be mounted within a diagnostic box between two cryomodules, with inner aperture that approximately matches the limiting beam aperture in the cryomodule. Tests of the loss ring sensitivity were performed at the National Superconducting Cyclotron Laboratory. The FRIB loss ring design and measured sensitivity are shown in Fig. 24.
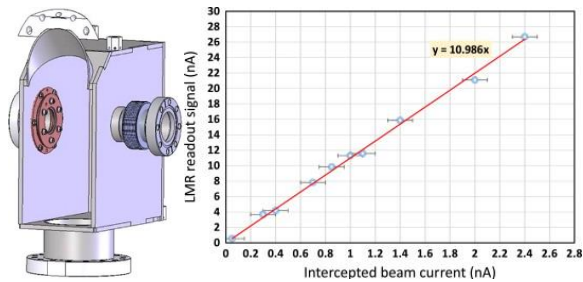

Figure 24: Installation and measured sensitivity of loss monitor ring. [13].

A comparison (Table 3) of the detected signal between the loss ring and the SNS ion chamber was made, in the case of uniform 1 W/m loss of uranium ions in the FRIB linac.

Table 3: Performance Comparison between Loss Monitor Ring and Ion Chamber. [13]

Loss Mode	Loss Source Location	^{238}U Energy / Charge [(MeV/u) / Q]	Loss Level [W/m]	Ion Chamber Signal [pA]	HMR Intercepted Beam [nA]
Slow loss	LS1	10 / 33+	1	0.003 *	72 **
	LS2	60 / 78+	1	0.3 *	29 **
	LS3	200 / 78+	1	4.2 ***	9 **
Fast loss	3rd ↕=0.29 cavity	20 / 78+	~1300 (in ~15m)	~7.0	29×10^3

* Assume the transfer function of ion chamber is 16.9 pA/R/hr (SNS).
** Assume HMR intercepts 1 W/m × 5 m beam power.
*** LS3 signal is calculated from loss in a superconducting structure.

A similar halo ring is currently employed at the PSI Ultra-Cold Neutron source beamline [50]. This implementation is segmented into 4 quadrants, with individual readouts. The signals are read and compared to a nearby current monitor. With proper tuning and collimation, the halo monitor should indicate 5% beam current interception.

An obvious criticism of employing intercepting devices near SRF cryomodules is the risk of material sputtering, beam scattering, and gas production due to primary beam ion collisions. Calculation of the time required to sputter Nb ring atoms onto the surface of a Nb cavity to the London penetration depth is in excess of 10^5 years. Recent studies of tungsten, niobium, and carbon wire sublimation close to superconducting cavities at SPIRAL-2 [51] have shown encouraging results for tungsten and niobium bursts, while burst of carbon led to clear quenches.

LAYERED DESIGN ASPECTS

Machine protection system diagnostics exhibit various sensitivities and time response to beam losses incurred along an accelerator chain. To mitigate risk and increase the probability of a robust detection scheme, a network of sensors is established. As previously discussed, existing machines utilize complementary beam loss monitors to improve dynamic range in high loss regions, and incorporate beam intensity difference measurements alongside traditional radiation loss detectors. Responsiveness to losses occurring over multiple time scales permits optimization of specific device or technique sensitivity to losses on particular time scales. Specific scales are chosen to overlap with physical or administrative time scales of greatest concern.

The loss monitor network scheme for FRIB is shown in Table 4. Fast and slow losses, in each segment of the accelerator chain, are separated, and the primary as well as backup detection schemes are indicated. At low energy, the primary fast detection schemes are based on direct beam monitoring, with secondary radiation monitoring appearing only as the primary beam energy increases to a suitable production threshold. The slow loss schemes are based on time averaged loss ring monitoring as well as thermal drift monitoring in cryomodules.

Table 4: FRIB Beam Loss Detection Layers

		LS1	FS1	LS2 low energy	LS2 high energy	FS2	LS3	BDS
Fast Loss	Primary	DBCM	DBCM	DBCM	DBCM	DBCM	DBCM	DBCM
< 35 μs	Secondary	HMR	HMR	HMR	BLM	BLM	BLM	BLM
	Tertiary				HMR	HMR	HMR	
Slow loss	Primary	HMR/Temp	HMR	HMR/Temp	BLM	BLM	BLM	BLM
> 100 ms	Secondary	HMR/Temp		HMR/Temp	HMR/Temp	HMR	HMR/Temp	
	Tertiary	Cryo		Cryo	HMR/Temp		HMR/Temp	
					Cryo		Cryo	

The LHC beam loss monitoring system is captured in the digital processing with 12 separate time scales extending from ½ turn (39 μs) to 84 s.

The layering of machine protection diagnostics and time scales with decision and control processes for SPIRAL-2 is shown in Fig. 25.
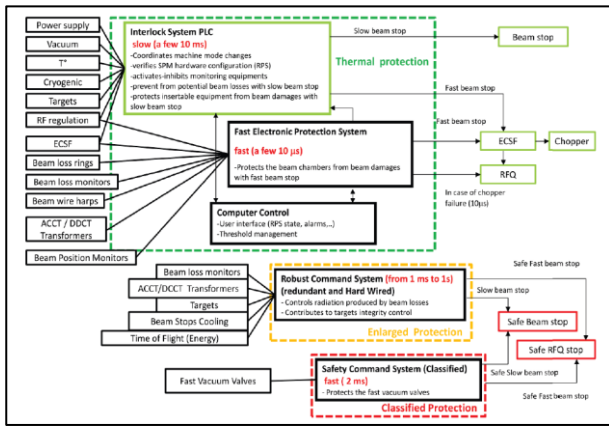
Figure 25: Components and layering of SPIRAL-2 machine protection system.[44].

SUMMARY

Elements of modern machine protection systems for high intensity hadron accelerators have been presented, emphasizing the types of diagnostic systems used and measurements that are required for a robust system.

ACKNOWLEDGMENT

REFERENCES

[1] J. Wei, "The very high intensity future," Proceedings of IPAC2014, MOYBA01, http://www.JACoW.org

[2] J. Wenninger, "State-of-the-art and future challenges for machine protection systems," Proceedings of IPAC2014, FRXCA01, http://www.JACoW.org

[3] J. Wenninger, Special CERN CAS, Feb. 2009.

[4] R. Schmidt, CAS, October 2011.

[5] http://www.srim.org/

[6] Y. Zhang, et al., "Analysis of beam damage to FRIB driver linac," Proceedings of SRF2011, MOPO058, http://www.JACoW.org

[7] H. Takei and H. Kobayashi, J. Nucl. Sci. Tech. 42, (2005), p. 1032.

[8] www.ansys.com

[9] D. Gassner, et al., "Spallation Neutron Source Beam Loss Monitor System," Proceedings of the 2003 Particle Accelerator Conference, p. 2447, http://www.JACoW.org

[10] R.A. Hardekopf, "Beam loss and activation at LANSCE and SNS," LA-UR-99-6825, Los Alamos National Laboratory, Los Alamos, NM, Sept. 1999.

[11] J. Galambos, et al., "Increased understanding of beam losses from the SNS linac proton experiment," Proceedings of LINAC2012. MO2A02; http://www.JACoW.org

[12] Z. Liu, et al., "Beam loss monitor system for the low-energy heavy-ion FRIB accelerator," Proceedings of IBIC2013, MOPC46; http://www.JACoW.org

[13] Z. Liu, et al., "A new beam loss monitor for low-energy protons and heavy-ion accelerators," Nucl. Instrum. Methods Phys. A, in press (2014).

[14] Geant4 collaboration, "Geant4 Simulation Toolkit," http://geant4.web.cern.ch/geant4

[15] A. Zhukov, "Beam loss monitors (BLMs): Physics, simulations, and applications in accelerators," Proceedings of BIW10, THTNB01 (2010).

[16] V.E. Weisskopf and D.H. Ewing, Phys. Rev. 57, 472 (1942).

[17] ENDF/B-VI Summary Document, Report BNL-NCS-17541 (ENDF-201) (1991), P.F. Rose ed., National Nuclear Data Center, Brookhaven National Laboratory, Upton, NY, USA.

[18] A. Fasso, A. Ferrari, J. Ranft, et al., "FLUKA: a Multi-Particle Transport Code," CERN-2005-10 (2005), INFN/TC_05/11, SLAC-R-773.

[19] Koji Niita, Tatsuhiko Sato, Hiroshi Iwase, et al., "PHITS - a Particle and Heavy Ion Transport Code System," Radiation Measurements 41 (2006) 1080.

[20] N.V. Mokhov, "The Mars Code System User's Guide", Fermilab-FN-628 (1995).

[21] http://mcnp.lanl.gov

[22] M. Stockner, "Beam Loss Calibration Studies for High Energy Proton Accelerators," CERN-THESIS-2008-009, (2008).

[23] M.Stockner, et al., 2006 IEEE Nuclear Science Symposium, N30-274, 1342-1345, (2006).

[24] L. Tchelidze, "Beam loss monitoring at the European Spallation Source," Proceedings of IBIC 2013, WEPC45; http://www.JACoW.org

[25] M. Jarosz, "Studies into beam loss patterns at European Spallation Source," Proceedings of IPAC2014, THPME165; http://www.JACoW.org;

[26] Q. Zhao, et al., "FRIB accelerator beam dynamics design and challenges," Proceedings of HB2012, WEO3B01 (2012).

[27] R. Bruce, et al., "Simulations and measurement of beam loss patterns at the CERN Large Hadron Collider," PR-STAB 17, 081004, (2014).

[28] A. Hofler, et al., "Innovative applications of genetic algorithms to problems in accelerator physics," PR-STAB 16, 010101, (2013).

[29] R.L. Witkover and D. Gassner, "Design of an improved ion chamber for SNS," BIW2002, AIP Conf. Proc. 648, (2002), p. 337.

[30] E.B. Holzer, et al., "Beam loss monitoring system for the LHC," IEEE-MIC '05, Puerto Rico, CERN-AB-2006-009 BI, (2005).

[31] D. Kramer, "Design and implementation of a detector for high flux mixed radiation fields", CERN-THESIS-2008-090, (2008).

[32] D. Kramer, *et al.*, "Secondary electron emission beam loss monitor for LHC", Proceedings of DIPAC 2007, WEPC03; http://www.JACoW.org

[33] M. Nikl, "Scintillation detectors for x-rays", Meas. Sci. Technol. **17** (2006) R37-R54.

[34] A. Zhukov, private communication.

[35] C. Kurfuerst, *et al*., "Investigation of the use of silicon, diamond, and liquid helium detectors for beam loss measurements at 2 Kelvin," Proceedings of IPAC2012, TUOAB02; http://www.JACoW.org

[36] C. Kurfuerst, *Cryogenic Beam Loss Monitoring for the LHC*, CERN-THSIS-2013-232, (2013).

[37] A. Warner, private communication.

[38] D. Orris, *et al.*, "Fast thermometry for superconducting rf cavity testing," Proceedings of PAC07, WEPMN105; http://www.JACoW.org

[39] J. Knobloch, *et al.*, Rev. Sci. Instrum. 65, 3521 (1994).

[40] J. Ozelis, private communication.

[41] S. Leloir, *et al*., "Measurement and control of the beam intensity for the SPIRAL-2 accelerator," Proceedings of IBIC2013, WEPF33; http://www.JACoW.org

[42] R.C. Webber, "Charged particle beam current monitoring tutorial," AIP Conf. Proc. 333, (1995), p. 3-23.

[43] W. Blokland, C. Peters, "A new differential and errant beam current monitor for the SNS accelerator," Proceedings of IBIC13, THAL2; http://www.JACoW.org

[44] M-H. Moscatello, *et al.*, "Machine protection system for the SPIRAL2 facility," Proceedings of IPAC2012, WEPPD044; http://www.JACoW.org

[45] H. Hassanzadegan, "Design, implementation and preliminary test results of the ESS beam current monitor system," Proceedings of IPAC2014, THPME160; http://www.JACoW.org

[46] S. Lidia, private communication.

[47] W. Blokland, private communication.

[48] R.E. Shafer, "Beam position monitor sensitivity for low-β beams," AIP Conf. Proc. 319, (1994), 303-308.

[49] O. Yair, *et al.*, "FRIB beam position monitor pickup design," Proceedings of IBIC2014, TUPF16 (2014).

[50] B. Blarer, *et al.*, "The beam safety system of the PSI UCN source," Proceedings of DIPAC2011, MOPD03; http://www.JACoW.org

[51] R.Ferdinand, *et al*., "Tests of wire sublimations very close to SPIRAL 2 superconducting cavity," Proceedings of LINAC08, THP005; http://www.JACoW.org